

FIG. 1: Characteristic IV of the narrow bridge used for the ARPES measurements. Three regimes are evident in the IV curve (1) At low currents below the de-pinning current no voltage is developed on the bridge. (2) Flux flows across the bridge and voltage is created (3) Above a certain current the system becomes unstable and the temperature increases rapidly due to the power dissipation. Inset: photo of the bridge and a schematic drawing of the device and the configuration of contacts.

were collected in the flux-flow regime. Further increasing the current eventually leads to instability and to a thermal run-away. A systematic measurement of the doping and temperature dependence of the critical current for the same Bi2212 bridges was published recently [10].

The samples were cleaved in the ARPES UHV-chamber at a pressure lower than 1×10^{-10} torr. To make sure that electrons are emitted only from the bridge area, where the current density is high, we used a very fine needle that was glued onto the bridge. Using these fine needles, we were able to cleave only the bridge without exposing any parts of the electrodes. We used a UV-laser as our photon source. Photon energy was set to 6.52eV and the laser was focused to a $\sim 100\mu\text{m}$ diameter spot. The advantage of using low-energy photons is the improved momentum resolution obtained; the drawback is the limitation in momentum range that can be mapped. Our setup enabled the measurement of the nodal region only. Each sample was measured at a temperature at which the de-pinning current was no more than 2mA.

Fig.2 presents the ARPES spectra of a bridge for three cases: No current, positive current of 4.8mA and negative current of 4.8mA. Very unusual behaviour is displayed: instead of the expected energy broadening, the spectra show an energy split, with no notable energy broaden-

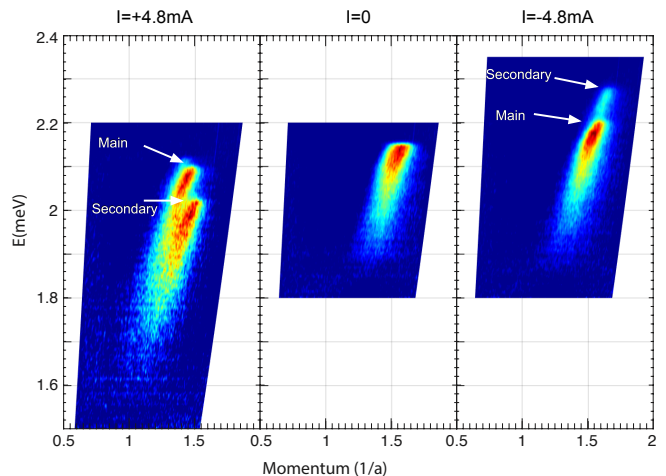


FIG. 2: ARPES spectra in the presence of current. Spectra with no current and with $\pm 4.8\text{mA}$ of current. In the presence of current, the spectrum is split into two distinct dispersions, which are shifted in energy. The dispersion that is shifted less with respect to the no-current dispersion is labeled "main", and the other dispersion is labeled "secondary".

ing. Although the definition of the Fermi level for each dispersion is unclear, a sharp edge is clearly discernable. The dispersion that is shifted less with respect to the no-current dispersion is labeled "main", and the other dispersion is labeled "secondary". When the current is reversed, the main and secondary dispersions exchange position. The energy difference between the two dispersions is about 100meV. In addition, the main dispersion is shifted slightly, by a few meV, relative to the Fermi level in the absence of current.

Next, we show data from a different sample as a function of current. The upper panel of Fig. 3 shows the ARPES spectra for several current densities. In this case the spectra are split into three parts. The energy difference between the different dispersions grows with the current density. The black symbols in the lower panel of Fig. 3 represent the energy difference between the main dispersion and the secondary dispersion for which the energy difference is maximal, as a function of the current. The red line is the IV curve measured during the ARPES measurement.

A perfect agreement is observed between the energy shift and the voltage drop across the bridge. This agreement suggests the following: for current densities larger than the de-pinning current density, vortices move through the bridge creating a voltage drop, but the flux flow is not uniform. Instead, the movement of vortices is restricted to narrow regions or channels. All of the voltage drop occurs in these channels, while most of the sample remains free of dynamic vortices and, as a result, free of phase fluctuations. In our experiment, the

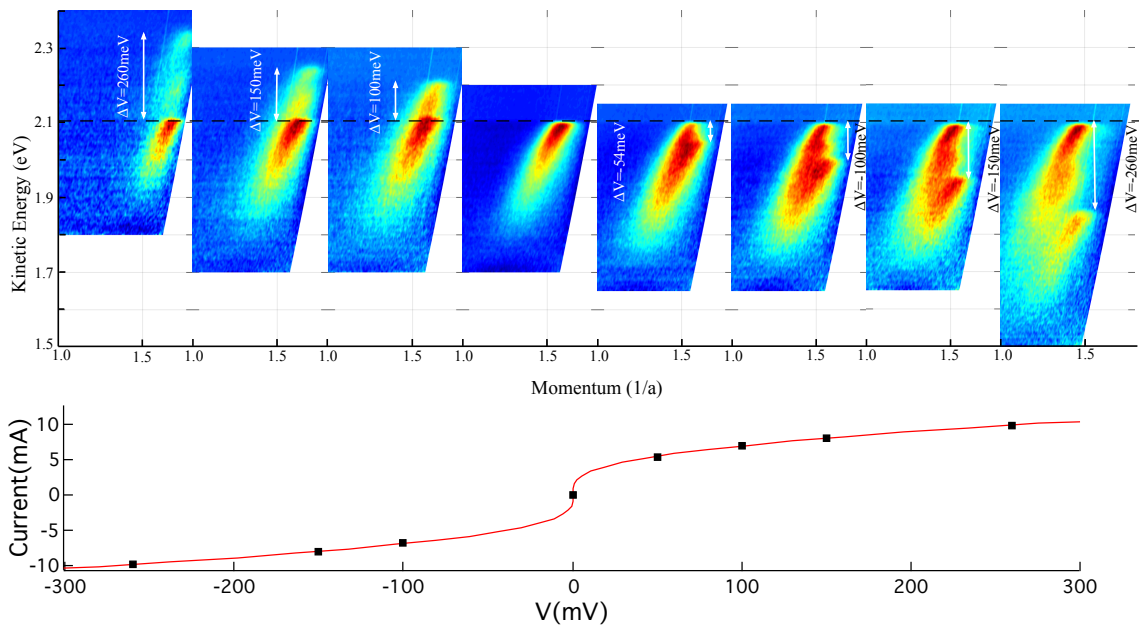


FIG. 3: Energy shift as a function of the current. The data is from a $T_c=62\text{K}$ underdoped sample, measured at $T=8\text{K}$. Upper panel: ARPES spectra for 8 different current values. The white arrows represent the energy shift between the intensity edges of the main dispersion and the most shifted secondary dispersion. Lower panel: the black squares represent the measured energy shift as a function of the current for the 8 current values shown in the upper panel. The red line is the IV curve for the same sample measured during the ARPES measurement.

large majority of electrons are emitted from these parts of the sample, as the flux channels occupy a negligible volume. In this flux-flow configuration, the chemical potential does not change linearly along the current direction but instead forms sharp steps and regions of constant chemical potential.

The chemical potential was measured at both ends of the bridge by measuring the Fermi edge of the Au contacts. The shift of the Fermi edge of the first contact with respect to the ground increases linearly with the current and is a result of contact resistance. This energy shift is identical to the energy shift of the main dispersion. The shift of the Fermi edge of the second contact equals the shift due to the contact resistance plus the shift due to the voltage drop across the bridge due to the flux-flow. We can fully reproduce the IV measurements using the photoemission from the Au contacts.

All of our sample exhibited the same behavior: some of the samples displayed two dispersions, other had three. In some samples there was no energy split, but even then there was no energy broadening; in those cases there is no flux flow in the cleaved area of the bridge but rather in other parts. We do not believe that the splitting of the spectra is unique to our samples. Indeed, a large body of literature exists that studied the morphology of the flux flow using many different techniques in many different samples. It seems that non-uniform flux flow is the rule

and not the exception [13].

The split in the spectra means that all phase fluctuations induced by the current are concentrated in a small part of the sample that was not probe in our ARPES experiment. These conditions create an opportunity to study SCs in the presence of very high current densities without any noticeable flux motion. Next, we describe the changes in the spectra as a result of the current.

Fig. 4(a) presents the momentum distribution curves (MDCs) for several current values obtained at an energy that corresponds to the position of the intensity edge of the main dispersion. These data were obtained along the nodal direction. It is clear to see that the peak in MDCs shifts away from the nodal point as the current increases. We also observe some broadening of the MDC peaks. The momentum shift in the main and secondary dispersions is identical, within our experimental error. These momentum shifts are quite significant, in Fig.4(b) we show the position of the MDC peak for different current values. For a current of about 10mA the momentum shift is about 10% of k_F .

Since current is being run through the sample, thus inducing a potential difference across the sample, we expect to have stray magnetic and electric fields in the vicinity of the sample. In the supplementary material section, we estimate these stray fields and show that their effect on the electron trajectories can account for no more than

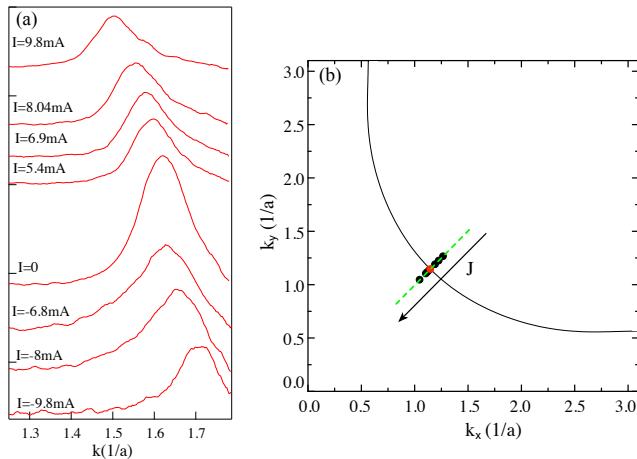


FIG. 4: Momentum shift. (a) The MDC at the intensity-edge energy for the main dispersion for several current values. The data was measured along the $\Gamma - Y$ direction. (b) Shift of the MDC peak for the same current values. The red point represents the node at zero current and the black line is the Femi-surface from a tight-binding calculation.

15% of the momentum shifts we observe. Moreover, a simple calculation shows that the magnetic field created by the current will deflect the electrons in the opposite direction to the direction found in the experiment. We therefore argue that most of the momentum shift is a result of the changes in the spectrum induced by the super-current.

Next we estimated the current density. Since the samples are cleaved, we would not use the cross-section of the bridge to calculate the current density, and so instead we used the critical current as a gauge. We measured carefully the doping and temperature dependence of the critical-current of a set of bridges for which we measured the cross section [10]. Since the de-pining current density is a fundamental property of the material, we assume that the cleaved bridges have the same critical current-density, which is measured in the ARPES chamber after cleaving. For currents larger than the de-pining current, the current flows uniformly through the narrow bridge [14]. Fig. 5 shows the shift in k_F as a function of the current density for 4 different samples. The shift is in the direction of the current. What is the origin of the observed momentum shift?

In the presence of a super-current the quasiparticle spectrum is Doppler shifted in a unique way [15]. The Bogoliubov spectrum is modified:

$$E^\pm(k, Q) = \frac{\xi_{k+Q/2} - \xi_{k-Q/2}}{2} \pm \sqrt{\left(\frac{\xi_{k+Q/2} + \xi_{k-Q/2}}{2}\right)^2 + \Delta(k)^2} \quad (1)$$

where ξ_k is the single particle dispersion. The Doppler

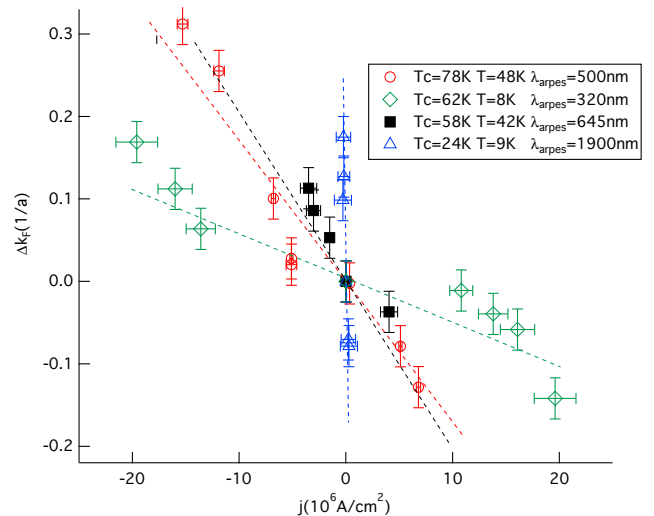


FIG. 5: Momentum shift as a function of current density for 4 different samples at different temperatures.

shift is momentum dependent and is proportional to the super-current wave vector, \vec{Q} , which represents the center-of-mass momentum of the pairs. Q is proportional to the current density. For a layered material such as Bi2212 it makes sense to use the 2D expression:

$$\vec{j} = \frac{e}{\hbar} \rho_s \vec{Q} \quad (2)$$

where \vec{j} is the current density and ρ_s is the superfluid stiffness of the SC.

For a d-wave SC, such as Bi2212, the Doppler shift will create particle and hole pockets around the nodal points depending on the current direction [3]. These pockets can be measured indirectly by measuring the magnetic-field dependence of the specific-heat of a d-wave SC. The magnetic field penetrates the SC in the form of a vortex lattice. The super-current circulating the vortex cores shifts the quasiparticles, creating pockets that contribute to the specific heat, a term that is proportional to \sqrt{H} [11]. This dependence, known as the Volovik effect, was measured in the cuprates [12].

For small values of Q along the nodal direction, we can rewrite Eq. 1 as:

$$E^\pm(k, Q) = v_F k \pm \frac{1}{2} v_F Q \quad (3)$$

where v_F is the Fermi velocity along the nodal direction. The size of the pocket created by the current along the nodal direction is Q . Eqs. 2 and 3 show that for a given current density, the size of the pocket is inversely proportional to the superfluid density, which depends on both the doping and the temperature.

It is tempting to think of the momentum shift we find as a direct measurement of the pocket size. The slope of

a linear fit to the data in Fig. 5 is given by $\frac{\hbar d}{2e\rho_0}$ where d is the c -axis lattice parameter of Bi2212. The penetration depth, λ , can now be calculated using the expression for the 2D superfluid stiffness:

$$\rho_0 = \frac{\hbar^2 d}{4\mu_0 e^2 \lambda^2}$$

The values we obtained are shown in the legend of Fig.5. These values are of the same order of magnitude as values found in measurements of the absolute value of the penetration depth of Bi2212 using different techniques [18–20].

Since the ARPES intensity is proportional to the spectral function, a better understating of the data requires that we consider the effect of the super-current on the spectral function. It was shown [6] that for small current densities and keeping only terms that are linear in Q , the spectral function in the presence of current can be written as $A_Q(\vec{k}, \omega) = A_0(\vec{k} - \vec{Q}, \omega - \frac{\hbar^2}{2m} \vec{k} \cdot \vec{Q})$, where A_0 is the spectral function without current. We see that in addition to the Doppler shift there is also a momentum boost, which completely cancels out the Doppler shift along the nodal direction, and so we should not expect a momentum shift at all along that direction [7].

A possible explanation for the observed shift are the interactions, which should not be neglected. Interactions can re-normalize the current carried by the quasiparticles by a factor α [16, 17], and so in Eq. 3 we should have, in fact, used the re-normalized term $\frac{1}{2}\alpha v_F Q$ to describe the Doppler shift. If $\alpha < 1$, the Doppler shift will no longer be cancelled by the momentum boost and k_F will be shifted. See the supplementary material for more details.

The London penetration depth as a function of the temperature and the doping level of the same Bi2212 films, was measured using a mutual inductance technique [21]. We found that the penetration depth extracted from the momentum shift was shorter than the values presented in Ref. [21]. The current re-normalization parameter can be estimated from the ratio of these values, $\alpha = 1 - (\frac{\lambda_{ARPES}}{\lambda_{London}})^2$. For the $T_c=78K$ sample we found $\alpha = 0.4 \pm 0.1$, for the moderately underdoped samples ($T_c=58K$ and $62K$) $\alpha = 0.6 \pm 0.1$, and for the extremely underdoped sample we find a very small value of $\alpha = 0.1 \pm 0.1$ was obtained. The results are in reasonable agreement with theory [3, 22] and with experimental estimates [23, 24].

Fig. 5 also reveals that for all of the samples shown, the dependence of the momentum shift dependence on the current density is not exactly linear; for high current densities it seems that $\frac{dk_F}{dj}$ increases, indicating that the superfluid density decreases. This is in agreement with theory [3, 4], which predicts that $\rho_s = \rho_0 - \frac{2\alpha^3 v_F^2}{\pi v_\Delta} Q$. In the present experiment we were not able to reach the critical current density at which ρ_s is expected to vanish, as this would require increasing the current density by an

order of magnitude. We hope to accomplish this in the future, using smaller bridges. In addition, all of the data presented is limited to the nodal direction; we hope in the future to be able to measure entire pockets by extending the momentum range we can cover.

We have shown that ARPES in the presence of current can be a useful way to understand the dynamics of flux in HTSCs and can be used to measure basic properties such as the super-fluid density and the current re-normalizaion parameter. We hope that our work will encourage others to measure different systems using similar methods.

This work was supported by the BSF, Grant No. 2010313. We acknowledge fruitful discussions with Lilach Goren, Ehud Altman, Erez Berg, Netanel Lindner and Boris Shapira.

-
- [1] A. Kanigel et. al. PRL **101** 137002 (2008).
 - [2] N Doiron-Leyraud et al. Nature **447** 565 (2007).
 - [3] Lilach Goren and Ehud Altman, PRB **79**, 174509 (2009).
 - [4] L.B. Ioffe, A.J. Millis, J. Phys. Chem. of Sol. **63**, 2259 (2002).
 - [5] V. J. Emery and S. A. Kivelson, Nature **374**, 434 (1995).
 - [6] M. Franz and A. J. Millis, Phys. Rev. B **58**, 14572 (1998).
 - [7] Erez Berg and Ehud Altman, PRL **99**, 247001 (2007).
 - [8] M. Khodas and A. M. Tsvelik, PRB **81**, 094514 (2010).
 - [9] A. Kaminski, et al., arXiv:1509.07937.
 - [10] Muntaser Naamneh, Juan Carlos Campuzano, and Amit Kanigel, PRB **90**, 224501 (2014).
 - [11] G. E. Volovik, JETP Lett. **58**, 469 (1993).
 - [12] K. A. moler et al. PRB **55**, 3954 (1997).
 - [13] Huebener R. P., *Magnetic Flux Structures in Superconductors*, Springer-Verlag Berlin (2010).
 - [14] Zeldov E. et al., PRB **49**, 9802 (1994).
 - [15] M. Tinkham, *Introduction to Superconductivity* Second Edition (Dover Books on Physics) (2004).
 - [16] A.J. Millis, S.M. Girvin, L.B. Ioffe, and A.I. Larkin, J. Phys. and Chem. Solids **59**, 1742 (1998).
 - [17] X.G. Wen and P.A. Lee, Phys. Rev. Lett. **80**, 2193 (1998).
 - [18] P. Zimmermann *et al.* Phys. Rev. **B52**, 541 (1995).
 - [19] O. Waldmann *et al.* Phys. Rev. **B53**, 11825 (1996).
 - [20] W. Anukool *et al.* Phys. Rev. **B80**, 024516 (2009).
 - [21] Jie Yong, MJ Hinton, Andy McCray, M Randeria, M Naamneh, A Kanigel, TR Lemberger, Phys. Rev. **B85**, 180507 (2012).
 - [22] C. P. Nave, D.A. Ivanov and P.A. Lee, Phys. Rev. **B73**, 104502 (2006).
 - [23] J. Mesot, M. R. Norman, H. Ding, M. Randeria, J. C. Campuzano, A. Paramekanti, H. M. Fretwell, A. Kaminski, T. Takeuchi, T. Yokoya, T. Sato, T. Takahashi, T. Mochiku, and K. Kadowaki, Phys. Rev. Lett **83**, 840 (1999).
 - [24] May Chiao, R. W. Hill, Christian Lupien, Louis Taillefer, P. Lambert, R. Gagnon, and P. Fournier, Phys. Rev. **62**, 3554 (2000).
 - [25] M.R. Norman, H. Ding, M. Randeria and J.C. Campuzano, Phys. Rev. **B57**, R11093 (1998).

SUPPLEMENTARY MATERIAL

Stray magnetic and electric fields

Running current through a sample will create electromagnetic fields in the vicinity of the sample and these can deflect the photo-electrons on the way to the analyzer. A full analysis of the electrons' trajectories in the vacuum chamber can be quite complicated and so we have estimated the contributions of the magnetic and electric fields separately. For the magnetic field we calculated the deflection of an electron leaving the sample in normal emission, at the analyzer entrance slit. We calculated the field of a slab $50\mu\text{m}$ wide, 200nm thick and 2mm long carrying 10mA , which is the highest current we used in the experiments. We ignored the return current reduces the magnetic field. We found that the deflection under such conditions is 0.8Deg for an electron with 2.1eV kinetic energy. This is less than 15% of the deflection we found in the experiment for the sample with the smallest deflection (largest superfluid stiffness).

Estimating the effect of the electric field created by the current is more difficult. There are no electric fields within the SC; fields can only develop across the vortex channels where there are sharp changes in the chemical potential. We used Simion to calculate the electron trajectories in the case of one such channel 1μ wide. We assumed the voltage across the channel is 300meV , larger than any voltage drop in our experiments. Simion solves the electron's equations of motion using specific boundary conditions. We used the real dimensions of the sample, chamber and electron analyzer. The maximal deflection for 2.1eV electrons was 0.6Deg , much smaller than the deflections we observed in the experiment.

To further test the direct effect of the current on the photo-electrons we conducted the following experiment: we prepared an optimally doped film and evaporated the 4 Au contacts on it. We did not, however, patterned it into a narrow bridge. The cross section of the film was 1000 larger than the cross section of the narrow bridge so we do not expect any momentum shift due to the low current density. We ran current through the film up to 60mA . The contact resistance was such that at 60mA the voltage that developed on the current contact was about 250meV at 60mA . The results are shown in Fig. S1.

In the upper part of the figure we show the raw detector images for zero current and for $\pm 60\text{mA}$. There is a shift in the dispersion when we plot the emission angle vs. kinetic energy. When the angle is translated to momentum, however, no change is seen in k_F of the node as a function of the current as shown in lower part of Fig. S1. The reason for the "disappearing" of the angular shift is the large shift in the kinetic energy.

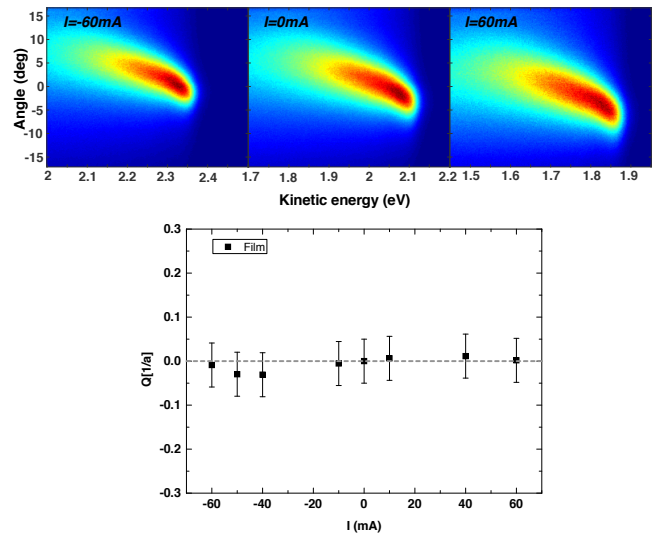


FIG. S1: Momentum shift as a function of the current for an un-patterned film.

Heating and temperature effects

All our measurements were done in the flux-flow regime where the samples are dissipative. The maximal power supplied during the ARPES measurements was $10\text{mA} \times 500\text{mV} = 5\text{mW}$, this is relatively low power compared with the cooling power of the LHe cryostat, which is well above 1W at these temperatures. Nevertheless, heat is transferred to the cold-finger through the insulating substrate, and temperature gradients can develop. Since we can run a real four-terminal measurement of the IV curve of the sample during the ARPES measurements, we know the exact temperature of the bridge during the experiments. Unlike a thermometer, which measures the temperature of the sample holder, the IV curve gives an accurate measurement of the temperature of the Bi2212 film itself. We did not find any significant change in the temperature during our measurements.

Fig. S2 presents data for a underdoped ($T_c=73\text{K}$) bridge measured at several temperatures. These measurements were done at different currents chosen such that the voltage across the bridge was 100meV . The split could be observed only below T_c , where even at $T=73\text{K} \sim T_c$ a small secondary dispersion can be observed. Several interesting things can be learned from this image: at 25K and 50K , deep inside the SC state, the energy difference between the main and secondary dispersion is the same, 100meV , which is the entire voltage drop across the bridge. Note that the position of the main dispersion is different because at 25K since more current is needed for the bridge to develop 100meV and this leads to a larger voltage drop on the current contact. At T_c , the energy difference between the dispersions is

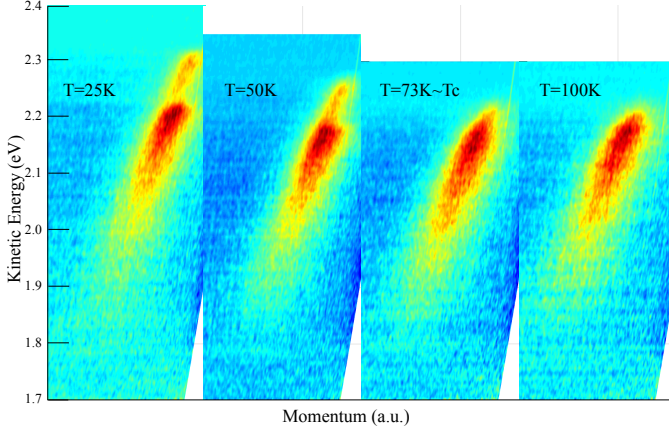


FIG. S2: Detector images for a $T_c=73\text{K}$ sample as a function of the temperature.

much smaller although the voltage across the bridge is the same, 100meV . The reason for this is that most of the resistance at T_c is not related to flux-flow but rather to normal parts of the sample. Above T_c , the sample is a plain resistor. The broadening due to the variation of the electro-chemical potential across the bridge is not significant. The 100meV develops across a $300\mu\text{m}$ bridge, so an emission spot of about $100\mu\text{m}$ will result in a broadening of no more than 30meV , which is consistent with our data.

Spectral function in the presence of current

The ARPES intensity is proportional to the spectral function that is given by the imaginary part of Green's

function. We use the usual BCS Green's function to calculate the spectral function:

$$G^{-1}(k, \omega)_0 = \omega - \varepsilon_k + i\Gamma - \frac{\Delta_k^2}{\omega + \varepsilon_k}$$

where ε_k is the tight-binding dispersion, Δ_k is the d-wave gap and Γ is a single-particle scattering-rate.

Using this approximation, the ARPES data may be fit below T_c [25] as was shown before. As shown by Franz and Millis [6] a uniform super-current will modify the Green's function as follows:

$$G_Q(k, \omega) = G_0(\vec{k} - \vec{Q}/2, \omega - \frac{\alpha\hbar^2}{2m}\vec{k} \cdot \vec{Q})$$

where α is current re-normalization parameter. The Doppler shift in d-wave superconductors creates particle and hole pockets. In Fig.S3 we show the spectral function at the Fermi level for the case where \vec{Q} is in the (π, π) direction. Panel (a) presents the spectral function, ignoring the momentum boost (without taking k to $k - Q$) for $\alpha = 1$. In this case we get pockets of size Q centred around the original nodes. The spectral weight is higher on one side of the pockets and, along the nodal direction in particular, the spectral weight vanishes on the "dark" side of the pockets. In Panel (b) we add the momentum boost, but maintain $\alpha = 1$. As can be seen, the center of the pockets is shifted by $Q/2$ leaving k_F of the "bright" side of the pockets exactly at the nodes. Panel (c) shows the spectral function for $\alpha = 0.5$; the result is smaller pockets of size αQ . Since the shift due to the momentum boost remains $Q/2$ we do observe a shift in k_F .

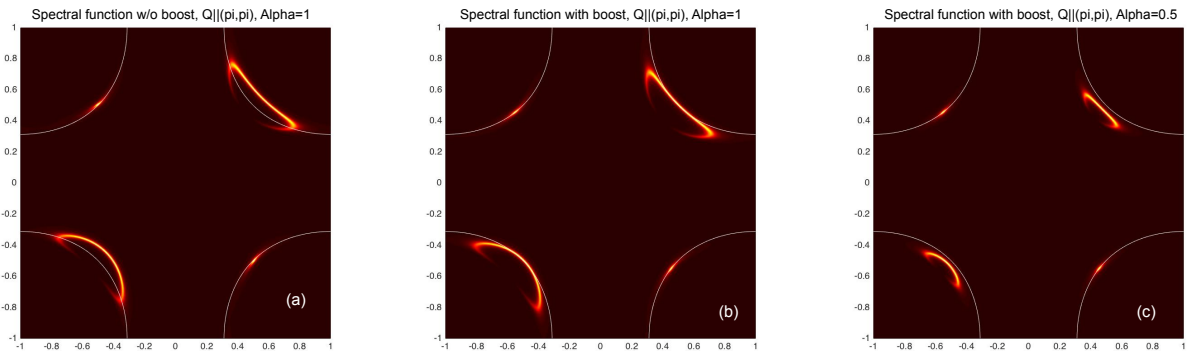


FIG. S3: The spectral function with current. (a) Calculation of the spectral function for the case of a current in the (π, π) direction with no momentum boost. (b) The same as (a) with the momentum boost. (c) The spectral function for the case of a re-normalized current ($\alpha = 0.5$).